Interplay of climate change-exacerbated rainfall, exposure and vulnerability led to widespread impacts in the Mediterranean region

Authors

1. Mariam Zachariah, *Grantham Institute, Imperial College London, UK*
2. Vassiliki Kotroni, *Institute of Environmental Research, National Observatory of Athens, Greece*
3. Lagouvardos Kostas, *Institute for Environmental Research and Sustainable Development, National Observatory of Athens, Greece*
4. Clair Barnes, *Grantham Institute, Imperial College London, UK*
5. Joyce Kimutai, *Grantham Institute, Imperial College London, UK*
6. Sarah Kew, *Royal Netherlands Meteorological Institute (KNMI), De Bilt, The Netherlands*
7. Izidine Pinto, *Royal Netherlands Meteorological Institute (KNMI), De Bilt, The Netherlands*
8. Nadia Bloemendaal, *Royal Netherlands Meteorological Institute (KNMI), De Bilt, The Netherlands*
9. Wenchang Yang, *Department of Geosciences, Princeton University, Princeton, NJ 08544, USA*
10. Maja Vahlberg, *Red Cross Red Crescent Climate Centre, The Hague, the Netherlands*
11. Roop Singh, *Red Cross Red Crescent Climate Centre, The Hague, the Netherlands*
12. Lisa Thalheimer, *United Nations University - Institute for Environment and Human Security, Bonn, Germany; Princeton School of Public and International Affairs, Princeton, USA*
13. Friederike Otto, *Grantham Institute, Imperial College London, UK*

Review authors

1. Sjoukje Philip, *Royal Netherlands Meteorological Institute (KNMI), De Bilt, The Netherlands*
2. Rana El Hajj, *Red Cross Red Crescent Climate Centre, The Hague, the Netherlands*
3. Celine El Khoury, *International Federation of Red Cross and Red Crescent Societies (IFRC), Geneva, Switzerland*
4. Sara Walsh, *International Federation of Red Cross and Red Crescent Societies (IFRC), Geneva, Switzerland*
5. Dominika Spyratou, *International Federation of Red Cross and Red Crescent Societies (IFRC), Geneva, Switzerland*
6. Eleni Tezapsidou, *International Federation of Red Cross and Red Crescent Societies (IFRC), Geneva, Switzerland*
7. Sanna Salmela-Eckstein, *International Federation of Red Cross and Red Crescent Societies (IFRC), Geneva, Switzerland*

8. Julie Arrighi, *Red Cross Red Crescent Climate Centre, The Hague, the Netherlands; Global Disaster Preparedness Center, Washington DC, USA; University of Twente, The Netherlands*

Main findings

- The severe flooding in Spain, Greece, Türkiye, Bulgaria and Libya was caused by very heavy rainfall that fell, in the case of Spain in less than 24 hours, whereas it lasted 24h in Libya and up to 4 days over Greece and Türkiye.
- For Libya and Spain, we thus evaluate the return period of the annual maximum of 1-day accumulated precipitation; for central Greece, and the larger region defined above the annual maximum of 4-day precipitation. As a summary assessment, we state that the return time for the event in Spain is a 1 in 10 to 1 in 40 year event;, for central Greece a 1 in 80 to 1 in 250 year event; for the large GBT region a 1 in 5 to 1 in 10 year event; and over Libya a 1 in 300 to 1 in 600 year event.
- In Libya the event magnitude is far outside that of previously recorded events.
- The uncertainties for the return times are very high and depend on the exact region and dataset chosen. In individual locations they can be very different from the ones shown here.
- To assess the role of climate change we combine observation-based products and climate models and assess changes in the likelihood and intensity of a 1 in 10 year 4-day event over the larger region encompassing Greece, and the parts of Türkiye and Bulgaria that were impacted by flooding, as well as the 1 in 600 year 1-day maximum rainfall event over Libya.
- For the large region including Greece and parts of Bulgaria and Türkiye, we find that human-induced climate change made an event as extreme as the one observed up to 10 times more likely and up to 40% more intense. An event as extreme as the one observed over Libya has become up to 50 times more likely and up to 50% more intense compared to a 1.2C cooler climate.
- The uncertainty in these estimates are high and encompass the possibility of no detectable change, but there are multiple reasons we can be confident that climate change did make the events more likely: from theory we know that an increase in rainfall intensity of around 10%, would be expected given current warming levels, so we could only report that there has been no change if there was a well known dynamic process counteracting this effect, which there is not. Studies focussing on extreme rainfall with future warming also show an increase in heavy rainfall, rendering it probable that the observed increase in heavy rainfall is indeed a trend due to climate change. For these reasons, we do not give a central estimate of the influence of climate change, as in previous studies, instead giving an upper-bound of the effect.
- In Greece, this has been a summer of extreme heatwaves and fires, and in the northeast of the country one of the largest fires ever recorded in the EU was burning as Storm Daniel devastated the centre of the country, stretching resources and limiting country-level response capabilities. Deforestation and relatively high rates of urbanisation have changed the landscape over time, increasing the number of people and assets exposed to flooding, and reducing stormwater drainage.

- In Libya, the volume of water and overnight timing of the dam failures meant that anyone in the path of the water was at increased risk, not just those who are typically highly vulnerable.
- Ongoing conflict and state fragility in Libya compounded the effects of the flooding, contributing to a lack of maintenance and deterioration of dam infrastructure over time and increasing people's risk and the resulting impacts. The conflict also limits nation-wide adaptation planning and coordination across a range of climate issues facing the country, such as water scarcity, and extreme weather including heat and floods.
- In addition to the lack of maintenance, the Al-Bilad and Abu Mansour dams were built in the 1970s, using relatively short rainfall records, and may not have been designed to withstand a 1 in 300 to 600 year rainfall event. A full after-action review looking at the design criteria of the dams will be required to understand the extent to which the dams' design, and the lack of subsequent maintenance contributed to the disaster. Even still, catastrophic dam failures and its impacts can be limited through risk reduction protocols that include real-time monitoring of forecasts, water volumes, and warning systems that alert those downstream of possible failures and the need to evacuate.
- While in Libya there was a forecast with a 3-day lead time on the track of Storm Daniel, the impact of that potential rainfall on infrastructure and people was not clearly understood in advance. Further, it is not clear to what extent forecasts and warnings were communicated and received by the general public, or relevant emergency responders. In conjunction with improved emergency management capacity, impact-based forecasts may help to provide a clearer understanding of how the rainfall translates into potential impacts and could lead to improved warnings in the future.
- This disaster also points to the challenge of needing to design and maintain infrastructure for not just the climate of the present or the past, but also the future. In Libya, this means taking into account the long-term decline in *average* rainfall, and at the same time, the increase in *extreme* rainfall like this heavy rainfall event; a challenging prospect especially for a country plagued by crises.

1 Introduction

During the first two weeks of September 2023 torrential rain fell in several countries across the Mediterranean, caused by low-pressure systems, notably storm "Daniel", forming around a blocking high centred over the Netherlands. The impacts began on the 3rd of September in Spain, when very heavy rainfall over a few hours led to floods in the central and southern parts of the country, killing at least five people. This episode was followed by very heavy rain that led to floods in central Greece and Bulgaria between the 4th and the 7th of September. Reports indicate that this storm, named Daniel by the Hellenic National Meteorological Service (CNN, 2023), is the worst to hit Greece since records began in 1930 (Reuters, 2023). At least 17 deaths were reported in Greece (Greek Herald, 2023), seven in Türkiye (Iran Front Page, 2023), six in Spain (France24, 2023), and four in Bulgaria

(Floodlist, 2023). The worst-affected region in Greece, the Thessaly plain, accounts for over one-quarter of the country's agricultural production (Politico, 2023). After more than 75,000 hectares were inundated, it is estimated that the agricultural sector in Thessaly will need five years to recover from the damages and for the lands to become fertile again (Le Monde, 2023). The last and the worst of the impacts of the storm was in northern Libya, where very extreme rainfall affected seven cities in the country. 3,958 fatalities have been confirmed in the city of Derna alone, and 170 people elsewhere in the country, while over 10,000 are still missing (CNN, 2023) following two dam breaks that caused four bridges and some multi-storeyed buildings to collapse on the night of the 10th (Aljazeera, 2023; Reuters; 2023). The devastating scale of impacts associated with the event is rendering it the deadliest and costliest storm over the Mediterranean and Africa, respectively, on record (Yale University, 2023). With Cyclone Freddy ranking second with approximately 1,400 fatalities (The Bureau of Meteorology, 2023), Storm Daniel is by far the deadliest extreme weather event of 2023 to date, and the deadliest storm worldwide since 2008 when over 130,000 lives were lost to Cyclone Nargis (Enz, 2009).

The positioning and intensity of the northern hemisphere jet stream led to the formation of an omega blocking pattern, trapping a high-pressure system between two low-pressure systems. The name Omega comes from a resemblance to the Greek letter Ω on a weather map (Figure 1). An omega block (three vortices) is a mid-tropospheric high-pressure system that lies polewards of one or two lows, characterised by widespread persistence with typically upward vertical velocity that enhances low level convergence and high level divergence that favours unstable atmospheric stability for extreme rainfall. Omega blocks have been associated with several extreme events including those that caused record-breaking floods downstream in Pakistan in 2011 (e.g. Hong et al., 2011), flash floods in large parts of western and central Europe in May 2018 (Mohr et al., 2020), extreme rainfall in Northwestern Iran in 2008 (Samakosh et al., 2012), the record-shattering 2010 heatwave (Di Capua e al., 2021), and exceptional heatwaves in 2019 May in France and July in Germany (Bissolli et al., 2019). The blocking disrupted the typical west-to-east progression of weather systems, resulting in stagnant weather conditions across Europe which consequently, led to heavy rainfall over the Iberian Peninsula, Greece, Bulgaria and Türkiye, as well as a late summer heatwave over France, the Benelux countries, and the UK.

The torrential rainfall over Spain originated from a stagnant low-pressure system which became detached from the jet stream, also known as a cut-off-low (COL). COLs are synoptic-scale baroclinic systems that can cause severe weather, heavy rainfall events and floods. On the 3rd of September the highest rainfall was recorded in Madrid (104.9mm in Villanueva de la Cañada), Toledo (91.8mm), Cádiz (172.2mm in San José del Valle) Castelló/ Castellón (83.2mm at La Pobla de Benifassà-Fredes). On 4th of September the highest rainfall was recorded in Madrid (72.1mm in Colmenar Viejo) and Cuenca (46.8mm in Belmonte) (all AEMET, 2023). The Madrid region experienced its worst rainfall since 1972 (CGTN, 2023).

Similarly, over Greece, Bulgaria and Türkiye the extreme rainfall occurred in connection with the slowly-moving low-pressure system, known as Storm Daniel, that formed on September 5th. The National Observatory of Athens (NOA) had categorised the rainfall over Greece as a category 5 event – the most severe category – two days before its onset, using their operational Regional Precipitation Index (RPI; developed by Lagouvardos et al., (2023)), which takes into account the distribution of forecasted rainfall, and the area and population in the Greek territory expected to be affected. The storm brought exceptionally heavy rainfall, reaching 760mm in Greece, marking a new national record for daily precipitation (Meteo.gr, 2023). The storm then moved back along the southern Ionian

Sea where it developed into a MEDIterranean hurriCANE - Medicane (Copernicus, 2023), making landfall on the Libyan coast in the early hours of the 10th with strong winds of 70-80 km/h (WMO, 2023). The Ionian Sea, situated between Sicily and Greece and extending southward to the coast of Libya, is among the regions where Medicanes' formation occurs frequently. The peak of Medicane activity occurs between September and January (Cavicchia et al., 2014). In the city of Derna 250mm of rain fell within a few hours, with 414.1 mm in Bayda and 240 mm in Marawah, according to the National Center of Meteorology in Libya (FloodList, 2023).

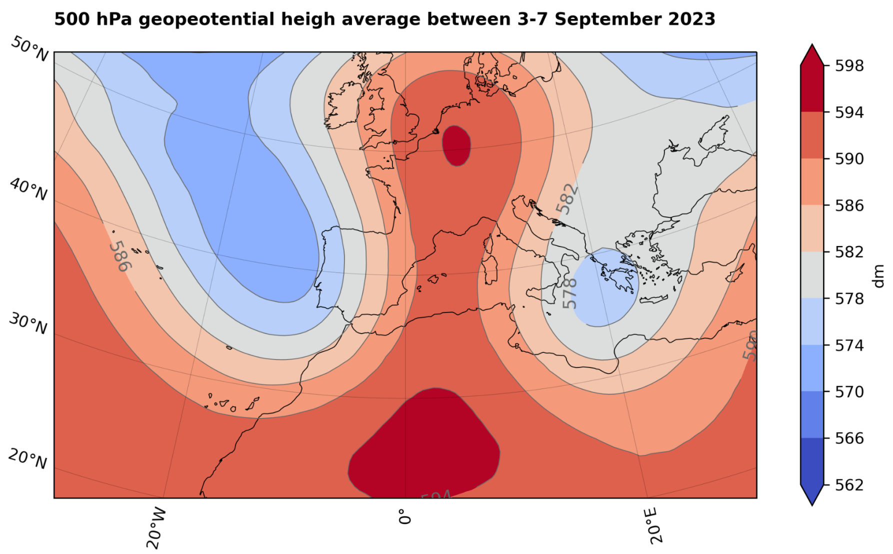

Figure 1: *Omega type of blocking pattern between 3-7 September 2023 (ERA5).*

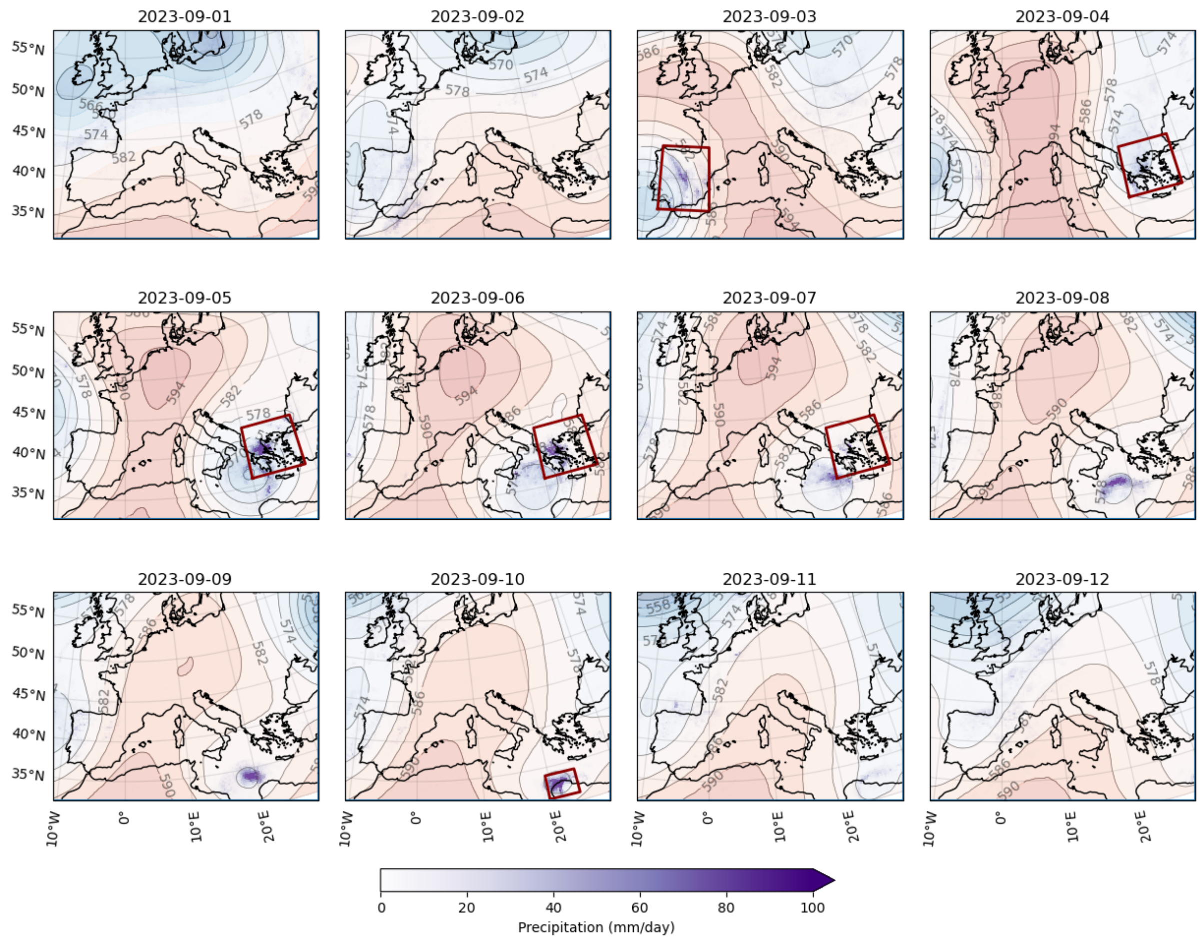

Figure 2*: 500 hPa geopotential height from September 1st-12th 2023, with daily accumulated precipitation overlaid (ERA5 analysis). Contours show 500 hPa geopotential height at intervals of 4 decameters. Red boxes indicate regions where heavy precipitation (shaded purple) and severe impacts were reported: central and southern Spain on September 3rd; Greece, Bulgaria and Türkiye from the 4th-7th; and Libya on the 10th.*

1.1 Event definition

The heaviest rainfall in Spain fell over a few hours, and so the true intensity of the event is not reflected by the 24-hour rainfall data that is most readily available and reliable in both gridded observational datasets and climate models (Berg et al., 2019; and references therein). It is thus not possible to undertake a robust quantitative attribution study using the multi-method probabilistic approach (Philip et al., 2020) for the rainfall event that led to the major flooding in Spain.

Over Greece and Bulgaria the precipitation fell within a four-day period, so the event is well represented in data products of daily resolution. This report therefore focuses on the larger-scale impacts of Storm Daniel across a large region encompassing the affected parts of these countries. Figure 2 shows the 4-day accumulated precipitation from the 4th to the 7th of September. The 4-day event definition also includes heavy precipitation in Bulgaria and northwestern Türkiye where major flooding affected the border cities of Tsarevo, Igneada and Arapya. The longer duration of the heavy rainfall in this part of the region allows for a more robust event attribution using the probabilistic approach. We therefore define the event for the remainder of the comprehensive attribution study as the maximum accumulated 4-day rainfall (Rx4day) in June-September (JJAS), averaged over land in the region 36 to 42.5N and 20 to 28.5 E, indicated by the red box in Figure 3 (hereafter, GBT box).

The last of the storm that made landfall in northern Libya on the 10th was characterised by heavy rainfall that was many times higher than the maximum rainfall in the region. For this event, we include a second definition: the annual (July-June) maximum rainfall (Rx1day), averaged over land in the region 32-33N and 20-23E, shown by the red box in Figure 4. We define the year from July to June because the rainfall cycle for this region is unimodal, peaking in January, and typically dry during JJAS. The intense local precipitation over Spain and Greece is also discussed briefly in Section 3.1.

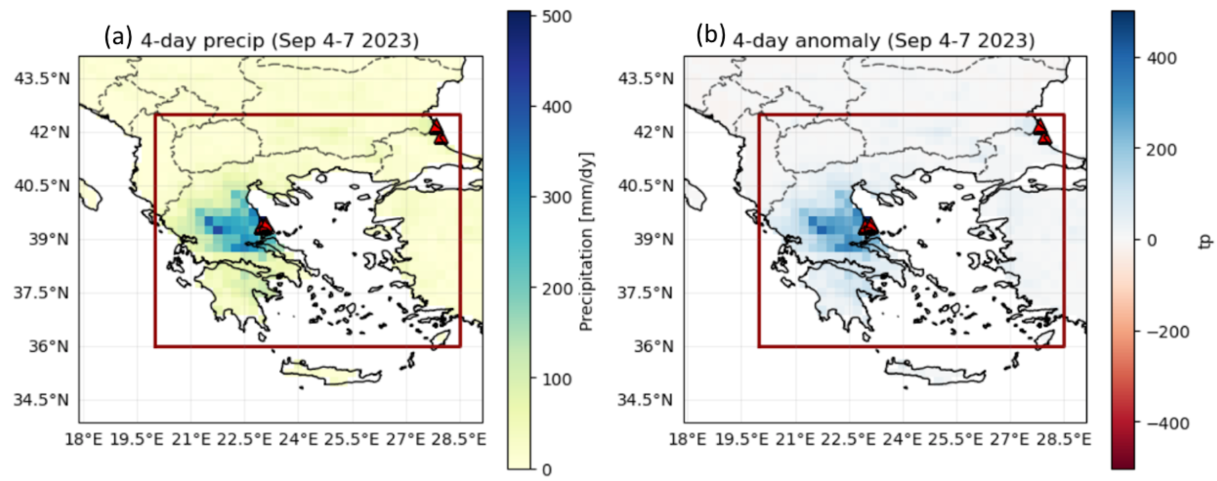

Figure 3: *(a) Observed maximum 4-day rainfall (Rx4day) during June-September (JJAS), in the year 2023, recorded on 4-7 September (ERA5). (b) same as (a), but as anomaly with respect to the climatological seasonal average for 1950-2023. The red triangles indicate cities with particularly severe impacts.*

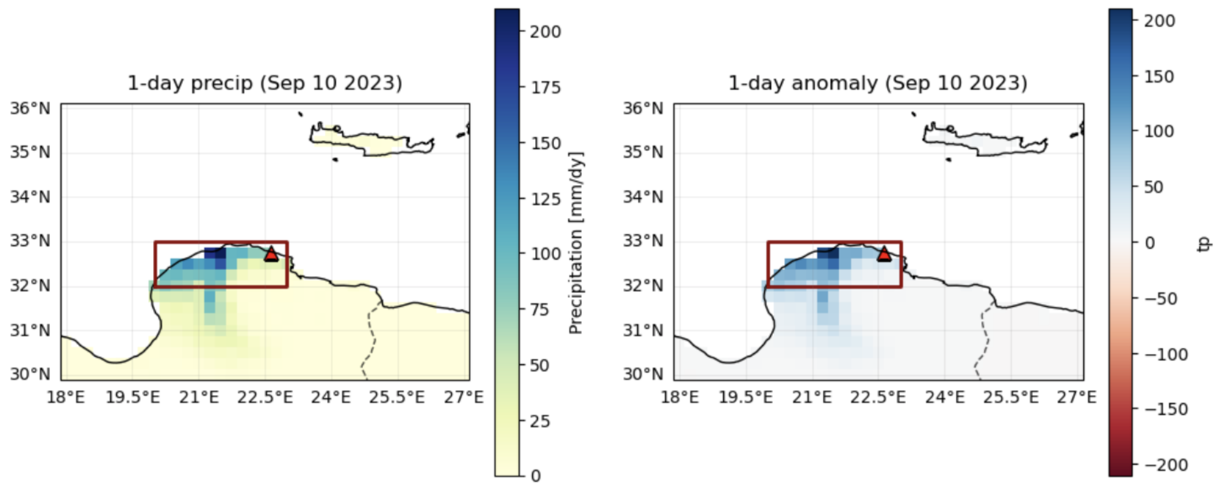

Figure 4: *(a) Observed annual maximum 1-day rainfall (Rx1d), in the year 2023, recorded on 10 September. (b) same as (a), but as anomaly with respect to the climatological seasonal average for 1950-2023. The red triangles indicate the port city of Derna where the impacts were particularly devastating.*

1.2 Past trends in Mediterranean rainfall extremes

The larger Mediterranean region of which Spain and the region around Greece and Libya are a part is one of the few regions in the world where there are many studies on observed precipitation trends and relatively abundant high-quality data, even though observed records are often comparably short. There are however different trends within the region with an increase in heavy rainfall in the more Northern parts, but no trends in the more Southern parts (Zittis et al., 2021) which leads to but no discernible signals in heavy precipitation for the region overall (Seneviratne et al., 2021). It has been shown that high internal variability masks the climate change signal in several parts of Europe (Kendon et al., 2023; Aalbers et al., 2017) thus leading to no, or smaller trends than expected from thermodynamics. A recent review of past and future trends in the Eastern Mediterranean region which encompasses the Greece region above, found locally observed increases in heavy precipitation while the trend only emerges for the whole region with warming from 1.5 C onwards (Zittis et al., 2022). Using precipitation time series from ERA5-Land, the National Observatory of Athens (NOA) estimated that Category 5 events (the most severe precipitation events) occurred once every year during 1991-2020, with 60% of days with precipitation of category 5 occurring in autumn, along with a statistically significant increasing trend in the number of events of Category 3 and higher (Lagouvardos et al., 2023). A study focussing on disentangling the thermodynamic from dynamic changes found that while the intensity in heavy precipitation events increases, the frequency decreases (Brogli et al., 2019). The results in this report are thus in line with previous assessments and in no contradiction to the IPCC reports, which also show the trends to emerge and become positive for the large Mediterranean region (Seneviratne et al., 2021) with future warming.

2 Data and methods

2.1 Observational data

Three gridded observational data products were analysed to estimate the amount of precipitation in the affected regions as well as weather station data over central Greece.

1. ERA5: The European Centre for Medium-Range Weather Forecasts, or the ERA5 reanalysis product begins in the year 1950 (Hersbach et al., 2020). We use reanalysis and analysis data from this product. It should be noted that the variables from ERA5 are not directly assimilated, but these are generated by atmospheric components of the Integrated Forecast System (IFS) modelling system. The re-analysis is available until the end of the preceding month (July 2023). We extend the re-analysis data with the ECMWF analysis (August up to the 10th of September).

2. MSWEP: The Multi-Source Weighted-Ensemble Precipitation (MSWEP) v2.8 dataset (updated from Beck et al., 2019) is fully global, available at 3-hourly intervals and at 0.1° spatial resolution, available from 1979 to ~3 hours from real-time. This product combines gauge-, satellite-, and reanalysis-based data.

3. CPC: The gridded product from NOAA PSL, Boulder, Colorado, USA known as the CPC Global Unified Daily Gridded data, is available at 0.5° x 0.5° resolution, for the period 1979-present. Data are available from NOAA.

4. NOA weather stations: The dense network of automatic weather stations in the area of Central Greece/Thessaly operated by NOA (Lagouvardos et al., 2017) is used in order to better assess the spatial and temporal resolution of rainfall accumulation in the flooded area during the event itself. 26 weather stations in Thessaly area provided observations of the precipitation during the event; these are visualised in Figure 6.

As a measure of anthropogenic climate change we use the (low-pass filtered) global mean surface temperature (GMST), where GMST is taken from the National Aeronautics and Space Administration (NASA) Goddard Institute for Space Science (GISS) surface temperature analysis (GISTEMP, Hansen et al., 2010 and Lenssen et al., 2019).

2.2 Model and experiment descriptions

We use three multi-model ensembles from climate modelling experiments using very different framings (Philip et al., 2020): Sea Surface Temperature (SST) driven global circulation high resolution models, coupled global circulation models and regional climate models, as well as the single coupled model ensemble FLOR.

1. Coordinated Regional Climate Downscaling Experiment (CORDEX) - European Domain (EURO-CORDEX) with 0.11° resolution (Jacob et al., 2014; Vautard et al., 2021). The ensemble used here consists of 23 simulations produced by combinations of six Global Climate Models (GCMs) and six Regional Climate Models (RCMs). These simulations are composed of historical simulations up to 2005, and extended to the year 2100 using the RCP8.5 scenario.

2. The FLOR (Vecchi et al., 2014), AM2.5C360 (Yang et al., 2021, Chan et al., 2021) and AM2.5 (Yang et al., 2021) climate models are developed at Geophysical Fluid Dynamics Laboratory (GFDL). The FLOR model is an atmosphere-ocean coupled GCM with a resolution of 50 km for land and atmosphere and 1 degree for ocean and ice. Ten ensemble simulations from FLOR are analysed, which cover the period from 1860 to 2100 and include both the historical and RCP4.5 experiments driven by transient radiative forcings from CMIP5 (Taylor et al., 2012). Both AM2.5C360 and AM2.5 are atmospheric GCMs based on that in the FLOR model (Delworth et al., 2012, Vecchi et al., 2014) with a horizontal resolution of 25 and 50 km, respectively. Three ensemble simulations of the Atmospheric Model Intercomparison Project (AMIP) experiment (1871-2100) from each of the two models are analysed. Radiative forcings are using historical values over 1871-2014 and RCP4.5 values after that. For each model, simulations are initialised from three different pre-industrial conditions but forced by the same SSTs from HadISST1 (Rayner et al., 2003) after groupwise adjustments (Chan et al., 2021) over 1871-2020. AM2.5C360 SSTs between 2021 and 2100 are using the FLOR RCP4.5 experiment 10-ensemble mean values after bias correction, while AM2.5 SSTs are using the first ensemble member values after bias correction.

3. CMIP6. This consists of simulations from 19 participating models with varying resolutions. For more details on CMIP6, please see Eyring et al., (2016). For all simulations, the period 1850 to 2015

is based on historical simulations, while the SSP5-8.5 scenario is used for the remainder of the 21st century.

4. HighResMIP SST-forced model ensemble (Haarsma et al., 2016), the simulations for which span from 1950 to 2050. The SST and sea ice forcings for the period 1950-2014 are obtained from the 0.25° x 0.25° Hadley Centre Global Sea Ice and Sea Surface Temperature dataset that have undergone area-weighted regridding to match the climate model resolution (see Table B). For the 'future' time period (2015-2050), SST/sea-ice data are derived from RCP8.5 (CMIP5) data, and combined with greenhouse gas forcings from SSP5-8.5 (CMIP6) simulations (see Section 3.3 of Haarsma et al. 2016 for further details).

2.3 Statistical methods

In this analysis we examine time series of JJAS Rx4day over the Greece and Bulgaria and Türkiye region, as well as annual RX1day over the Libya region defined in section 1.1. Methods for observational and model analysis and for model evaluation and synthesis are used according to the World Weather Attribution Protocol, described in Philip et al. (2020), with supporting details found in van Oldenborgh et al. (2021), Ciavarella et al. (2021) and here. The analysis steps in the protocol include: (i) trend calculation from observations; (ii) model evaluation; (iii) multi-method multi-model attribution and (iv) synthesis of the attribution statement. To statistically model both of the events under study, we use a nonstationary GEV distribution in which the location parameter shifts with GMST, while the dispersion (the ratio of the standard deviation to the mean) remains fixed. We estimate the return period and change in intensity of the event in these nonstationary models, in order to compare the climate of the present and the climate of the past, defined respectively by the GMST values of 2023 and of a 1.2° cooler climate representing the preindustrial past (1850-1900, based on the Global Warming Index). 95% confidence intervals are estimated for all quantities by a nonparametric bootstrapping procedure. Typically, results from observations and models that pass the evaluation tests would be synthesised into a single attribution statement combining the observational and model results; however, as discussed in the next section, we are unable to do so in this case.

3 Observational analysis: return period and trend

3.1 Evaluation of local precipitation

As discussed in Section 1, impacts from precipitation associated with this blocking event were experienced across a wide area, from Spain in the west to Bulgaria in the east, and therefore this study examines precipitation over a large part of southern Europe, in order to understand the effect of climate change on large-scale precipitation like that associated with Storm Daniel. However, as will be seen in section 3.2, the precipitation over the larger study region taken as a whole was not particularly unusual; the observed impacts arose from very intense localised precipitation. We therefore also estimate the return time of precipitation over smaller regions where the most severe impacts were reported. The flooding in Bulgaria was related to short-duration (sub-daily) precipitation, but was not particularly unusual at the daily timescale, so is not included here. For

Spain, we evaluate the return period of the annual maximum of 1-day accumulated precipitation; for central Greece, we consider the annual maximum of both 2- and 4-day accumulated precipitation. Maps of the maximum accumulated precipitation during September 2023 in these subregions and at these timescales are shown in Figure 5. In all cases, only precipitation over land cells is included in the analysis.

How unusual the event was does not only depend on the exact region analysed but also on the observational data product. To estimate the sensitivities we thus estimate return times both using the 73-year ERA5 reanalysis and the shorter but higher-resolution MSWEP data product.

In central Spain, the 1-day accumulated precipitation on September 3rd was found to be a 37-year event (95% confidence: 16-172 years) in ERA5; the event was not found to be particularly extreme in MSWEP (best estimate: 6-year event, 3-15). However, analysis of 3-hourly data from the MSWEP dataset (not shown here) suggests that most of the precipitation fell in less than half a day; analysis of sub-daily precipitation is beyond the scope of this report.

Over the rectangular region of central Greece outlined in Figure 5, both the 2-day and 4-day precipitation observed were found to be more extreme in ERA5, with estimated return periods of 224 (53-1 million years) and 240 (46-452,000) respectively; in MSWEP, the 2-day rainfall registered as a 106-year event (19-692,000) and the 4-day rainfall as an 88-year event (17-386,000). Note that unlike the results in Section 3.2, which evaluate changes in precipitation between the months of June and September, these return periods are with respect to annual precipitation, reinforcing the extreme nature of the rain that fell in these smaller areas.

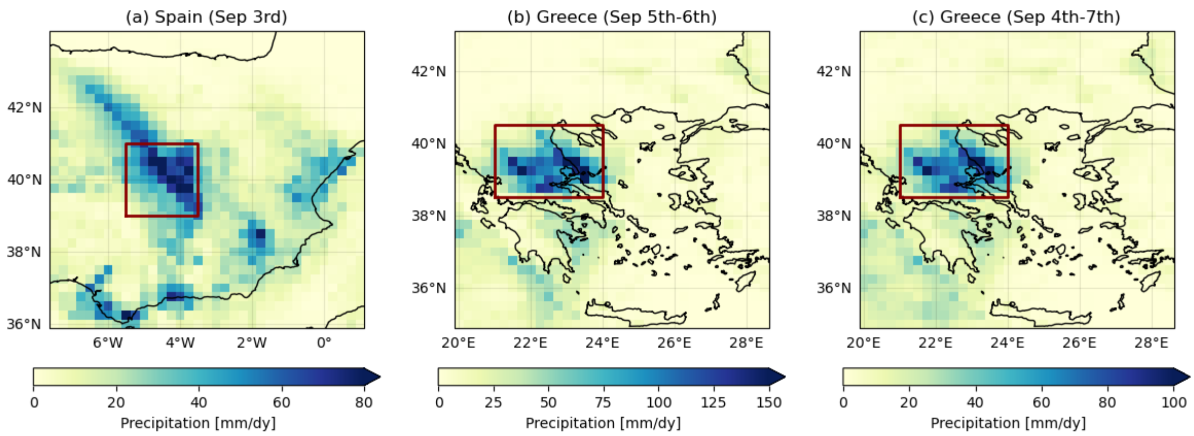

Figure 5*: Mean daily precipitation (ERA5) on the days on which the most extreme precipitation and flooding occurred. In each panel, the red box indicates the smaller region used to estimate the local return period. (a) 1-day accumulated precipitation over central Spain (5.5W-3.5W, 39N-41N); (b) 2-day accumulated precipitation over central Greece (21E-24E, 38.5N-40.5N); (c) 4-day accumulated precipitation over central Greece (21E-24E, 38.5N-40.5N)*

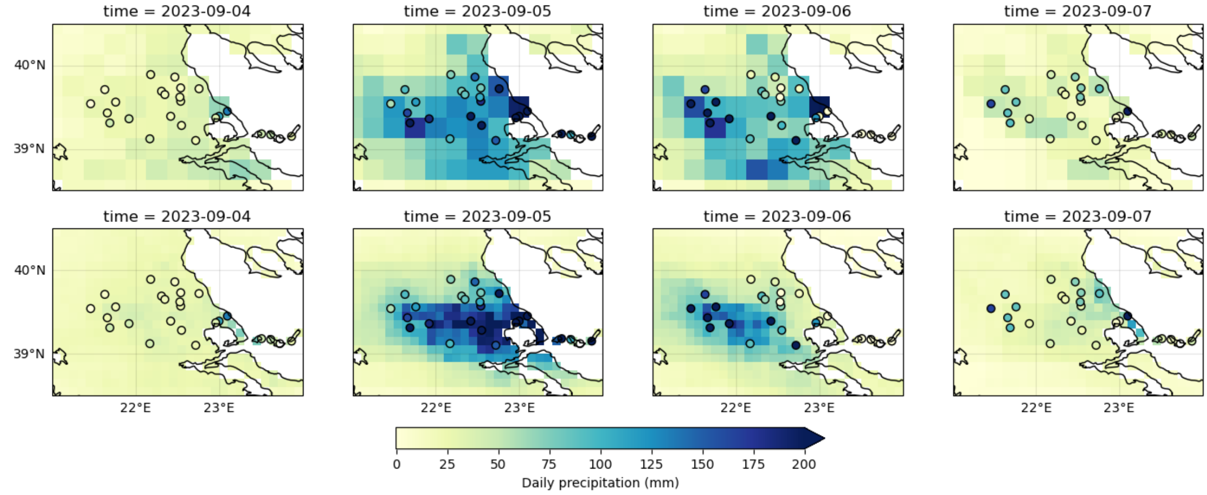

Figure 6*: Maps of daily precipitation from September 4th-7th in the region of central Greece bounded by the red box in Figure 5. Top row: ERA5; bottom row: MSWEP. Circles represent weather stations operated by the METEO/NOA within the heavily-impacted region of Thessaly where observations during Storm Daniel were available.*

To understand whether there are reasons to prefer MSWEP data over ERA5, despite the considerably shorter length of time over which MSWEP data is available (44 years, as opposed to the 73 years of ERA5 reanalysis), we compare both data sets to station data which is available over 26 stations in central Greece. The results are shown in Figure 6, where we see that the heavy rainfall in ERA5 has a larger spatial extent than the stations, whereas MSWEP has higher local intensities. These differences could explain the difference in return times which are very sensitive to magnitude. Given that the available station data records are too short to calculate return times this gives no strong indication that MSWEP is definitely more realistic than ERA5, even though the spatial extent of the event on the 6th is better captured in MSWEP. Furthermore, over the larger GBT region, the return period estimates from the two datasets are comparable, with a return period of ~5 years in MSWEP vs ~10 years in ERA5. Therefore, due to the short length of MSWEP we use the longer ERA5 dataset as our primary source for the observational analysis of Rx4day over the GBT region.

The event in Libya does not appear as particularly extreme in MSWEP (not shown), in contrast to all reports about the event and the nature of the rainfall; thus, ERA5 is the only available observation-based data set used in this analysis. We acknowledge that the uncertainties around the return times are very high. The fact that the event over Libya was well forecast (Severe Weather Europe, 2023) gives some confidence in using ERA5.

As a summary assessment: we state that the return time for the event in Spain is a 1 in 10 to 1 in 40 year event, for central Greece a 1 in 80 to 1 in 250 year event, for the large GBT region a 1 in 5 to 1 in 10 year event and over Libya a 1 in 300 to 1 in 600 year event. We use the higher return times for the remainder of the analysis, but note that the assessment of the role of climate change is largely independent of the region and return time of the event (see section 6).

3.2 Analysis of gridded data for the GBT region

Figure 7 shows the results from the trend-fitting methods described in Philip et al. (2020) applied to the ERA5 time series of Rx4day over the GBT box (see Figure 3). The left panel shows the variable as a function of the GMST anomaly, while the right panel shows GEV return period curves for this variable in the present 2023 climate (red lines) and a hypothetical past climate when the global mean temperature was 1.2°C cooler (blue lines). An increasing tendency of extreme rainfall is seen in both datasets as GMST increases (although this was not statistically significant), suggesting the need for detailed investigation of these trends with climate models. The return period of the 2023 event (Figure 7b) is around 13 years (uncertainty: 6-70 years). For the remainder of the analysis we evaluate changes in probability and intensity of a 1-in-10 year event.

The probability of a 4-day rainfall spell at least as intense as the 2023 event would have been much smaller in the pre-industrial climate, with the event now being around 5 times more likely in the ERA5 dataset with respect to the past 1.2°C cooler climate (uncertainty: 0.5-70). A 1-in-10-year event in the current climate is 30% wetter nowadays, compared to the past (uncertainty: 7% drier to 80% wetter).

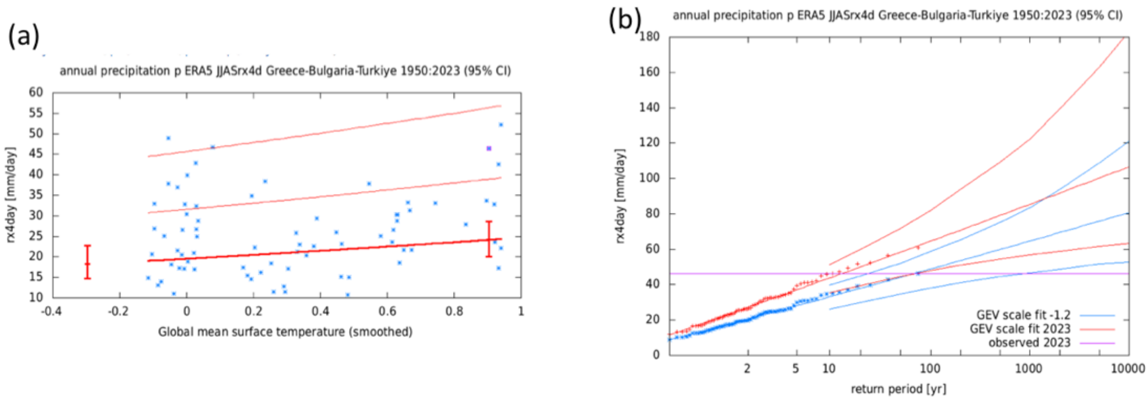

Figure 7: *Fitted trends and return level plots for a nonstationary GEV fitted to annual maxima of 4-day accumulated precipitation during June-September over the GBT box (ERA5).* ***(a)*** *Trend in annual maximum of 4-day rainfall as a function of the smoothed GMST. The thick red line denotes the time-varying location parameter and the thinner lines above represent the effective return levels of 6-year and 40-year events. The vertical red lines show the 95% confidence interval for the location parameter, for the 2023 climate and a 1.2ºC cooler climate. The 2023 observation is highlighted with the magenta box.* ***(b)*** *Return time plots for the climate of 2023 (red) and a hypothetical climate with 1.2ºC cooler GMST (blue). Points show the observed return levels against their expected return periods;the central line shows the fitted values, with the upper and lower lines showing a bootstrapped 95% confidence interval. The magenta line shows the magnitude of the 2023 event.*

3.3 Analysis of gridded data for northern Libya

Figure 8 shows the results from trend-fitting to Rx1day over the Libya region. The event on the 10th of September 2023 was many times higher than any single day of precipitation previously recorded in ERA5 (~70mm for the box in Figure 4). The event is estimated to be a 1-in-643 year event (uncertainty: 115 to 0.114E+10), and an even rarer event in the hypothetical, 1.2ºC cooler world with a return period of 1900 years (uncertainty: 237 to inf). In defining the event for the attribution analysis, we round the return period in the observed climate to 1-in-600. The best estimate for the probability ratio between now and the 1.2ºC cooler climate is 3 (uncertainty: 0.5 to 2100), with increase in intensity of the rainfall by 29% compared to in a 1.2º cooler past (uncertainty: 11% drier to 88% wetter).

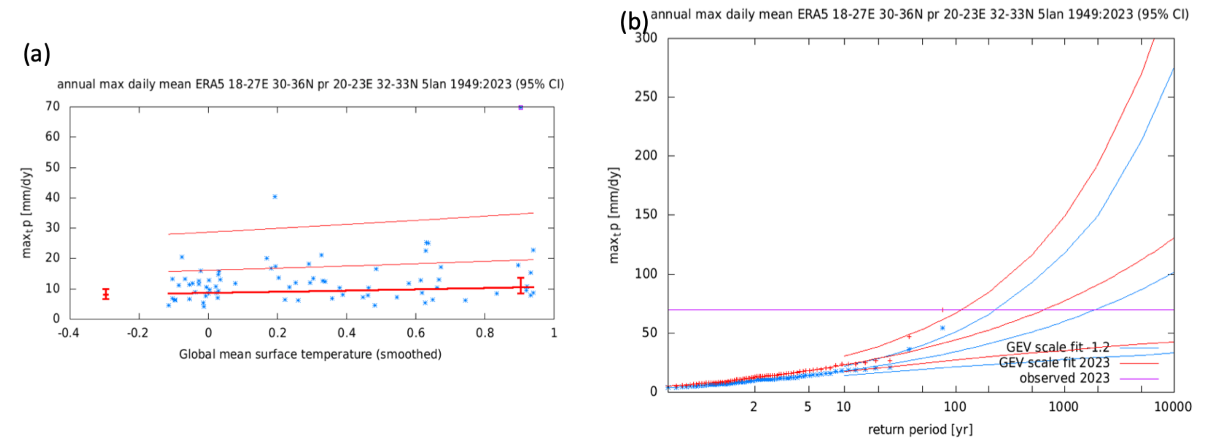

Figure 8: *Fitted trends and return level plots for a nonstationary GEV fitted to July-June annual maximum daily precipitation over northern Libya (ERA5).* ***(a)*** *Trend in annual maximum of 1-day rainfall as a function of the smoothed GMST. The thick red line denotes the time-varying location parameter and the thinner lines above represent the effective return levels of 6-year and 40-year events. The vertical red lines show the 95% confidence interval for the location parameter, for the 2023 climate and a 1.2ºC cooler climate. The 2023 observation is highlighted with the magenta box.* ***(b)*** *Return time plots for the climate of 2023 (red) and a hypothetical climate with 1.2ºC cooler GMST (blue). Points show the observed return levels against their expected return periods;the central line shows the fitted values, with the upper and lower lines showing a bootstrapped 95% confidence interval. The magenta line shows the magnitude of the 2023 event.*

4 Model evaluation

In the subsections below we show the results of the model evaluation for JJAS Rx4day for the GBT region (Table 1) and annual (July-June) Rx1day for the Libya region (Table 2). Models are evaluated over the 30-year period, 1980-2010. The climate models are evaluated against the observations in their ability to capture:

1. Seasonal cycles: For this, we qualitatively compare the seasonal cycle of daily precipitation in the study regions in the climate model outputs against the cycle computed from ERA5. We discard any models that exhibit ill-defined peaks in their seasonal cycles.

2. Spatial patterns: Models that do not match the observations in terms of the large-scale pattern of mean precipitation during JJAS (for GBT) and annually (for Libya) are excluded.

3. Parameters of the fitted GEV model: We discard the model if the 95% confidence intervals of the shape and dispersion parameters of the fitted GEV do not overlap with those estimated from the gridded observations.

The models are classified as ‘good’, ‘reasonable’, or ‘bad’ based on their performance in each of the three criteria discussed above. If the model is ‘good’ for all of these criteria, we give it an overall rating of ‘good’ (green highlight). We rate the model as ‘reasonable’ or ‘bad’, if it is rated ‘reasonable’ or ‘bad’, respectively, for at least one of the three criteria. These are respectively shown by the yellow and red highlights in the tables below. Where multiple realisations of the same

GCM-RCM pairing in the EuroCORDEX ensemble pass validation, only one is selected for inclusion in the final analysis. If five models or fewer are classified as ‘good’ in any ensemble, we also include models that only just pass the evaluation tests (classified as ‘reasonable’) for that model setup.

4.1 For GBT region

Table 1*: Evaluation results for the climate models considered for the attribution analysis of the maximum 4-day accumulated rainfall in the JJAS season for the GBT study region. The table contains qualitative assessments of seasonal cycle and spatial pattern of precipitation from the models (good, reasonable, bad) along with estimates for dispersion parameter, and event magnitude. The corresponding estimates for the ERA5 dataset is shown in blue. Based on overall suitability, the models are classified as good, reasonable or bad, shown by green, yellow and red highlights, respectively.*

Observations	**Seasonal cycle**	**Spatial pattern**	**Dispersion**	**Shape parameter**	**Event magnitude**
ERA5			0.357 (0.298 ... 0.404)	0.012 (-0.20 … 0.18)	
Model					**Threshold for 1-in-10 year event**
CMCC-CM2-HR4 SST-present (1)	good	reasonable	0.379 (0.288 ... 0.460)	-0.36 (-0.055 ... -0.085)	32.809
CNRM-CM6-1-HR SST-present (1)	good	good	0.329 (0.240 ... 0.410)	-0.13 (-0.96 ... 0.040)	79.213
HadGEM3-GC31-MM SST-present (1)	good	good	0.327 (0.254 ... 0.388)	-0.18 (-0.49 ... 0.034)	25.003
MPI-ESM1-2-HR SST-present (1)	good	reasonable	0.488 (0.344 ... 0.615)	-0.16 (-0.038 ... 0.081)	33.938
FLOR historical-rcp4.5 (10)	good	reasonable	0.276 (0.261 ... 0.290)	-0.091 (-0.14 ... -0.050)	36.856
AM2.5C360 amipHistorical+rcp4.5SST (3)	good	reasonable	0.336 (0.298 ... 0.367)	-0.18 (-0.28 ... -0.096)	38.743
AM2.5 amipHistorical+rcp4.5SST (3)	good	reasonable	0.347 (0.309 ... 0.379)	0.044 (-0.065 ... 0.14)	37.589
CNRM-CM5_r1_ALADIN53 Historical-rcp85 ()	bad	bad	0.189 (0.141 ... 0.229)	-0.17 (-0.47 ... 0.037)	40.606
CNRM-CM5_r1_ALARO-0 Historical-rcp85 ()	bad	reasonable	0.235 (0.169 ... 0.285)	-0.16 (-0.52 ... 0.12)	45.712
CNRM-CM5_r1_CCLM4-8-17 Historical-rcp85 ()	reasonable	reasonable	0.224 (0.147 ... 0.275)	-0.0082 (-0.41 ... 0.63)	42.986
CNRM-CM5_r1_RACMO22E Historical-rcp85 ()	reasonable	reasonable	0.289 (0.220 ... 0.339)	-0.011 (-0.27 ... 0.18)	45.841
CNRM-CM5_r1_REMO2015 Historical-rcp85 ()	bad	reasonable	0.266 (0.172 ... 0.335)	-0.00062 (-0.31 ... 0.27)	38.962
EC-EARTH_r1_RACMO22E Historical-rcp85 ()	good	reasonable	0.367 (0.282 ... 0.427)	-0.010 (-0.40 ... 0.37)	28.233
EC-EARTH_r3_COsMO-crCLIM-v1-1 Historical-rcp85 ()	good	good	0.397 (0.272 ... 0.483)	0.0080 (-0.31 ... 0.50)	27.203
HadGEM2-ES_r1_COsMO-crCLIM-v1-1 Historical-rcp85 ()	good	reasonable	0.435 (0.293 ... 0.523)	-0.11 (-0.39 ... 0.39)	33.823

HadGEM2-ES_r1_RACMO22E Historical-rcp85 ()	good	reasonable	0.459 (0.326 ... 0.537)	0.077 (-0.19 ... 0.40)	32.8627
IPSL-CM5A-MR_r1_REMO2015 Historical-rcp85 ()	bad	reasonable	0.326 (0.252 ... 0.390)	-0.32 (-1.0 ... 0.042)	26.632
MPI-ESM-LR_r1_RACMO22E Historical-rcp85 ()	good	reasonable	0.451 (0.333 ... 0.547)	-0.20 (-0.47 ... -0.029)	35.824
MPI-ESM-LR_r1_REMO2009 Historical-rcp85 ()	good	reasonable	0.368 (0.263 ... 0.448)	-0.20 (-0.74 ... 0.068)	36.174
MPI-ESM-LR_r2_COsMO-crCLIM-v1-1 Historical-rcp85 ()	good	reasonable	0.493 (0.393 ... 0.567)	0.11 (-0.51 ... 0.38)	31.704
MPI-ESM-LR_r3_REMO2015 Historical-rcp85 ()	reasonable	reasonable	0.384 (0.300 ... 0.434)	0.010 (-0.31 ... 0.25)	36.474
NorESM1-M_r1_ALADIN63 Historical-rcp85 ()	good	bad	0.479 (0.362 ... 0.562)	-0.026 (-0.34 ... 0.22)	42.596
NorESM1-M_r1_COsMO-crCLIM-v1-1 Historical-rcp85 ()	reasonable	reasonable	0.414 (0.318 ... 0.511)	-0.25 (-1.0 ... -0.036)	39.09
NorESM1-M_r1_RACMO22E Historical-rcp85 ()	good	reasonable	0.397 (0.286 ... 0.504)	-0.21 (-1.0 ... -0.062)	31.85
NorESM1-M_r1_REMO2015 Historical-rcp85 ()	bad	reasonable	0.329 (0.220 ... 0.397)	-0.15 (-0.45 ... 0.058)	30.454
ACCESS-CM2 Historical-ssp585 ()	good	reasonable	0.414 (0.325 ... 0.494)	-0.16 (-1.0 ... 0.24)	42.862
ACCESS-ESM1-5 Historical-ssp585 ()	reasonable	bad	0.413 (0.317 ... 0.537)	-0.14 (-1.1 ... 0.44)	49.031
CanESM5 Historical-ssp585 ()	reasonable	bad	0.492 (0.374 ... 0.570)	0.31 (0.076 ... 0.75)	19.593
CMCC-ESM2 Historical-ssp585 ()	good	bad	0.334 (0.253 ... 0.421)	-0.099 (-1.0 ... 0.27)	31.962
CNRM-CM6-1-HR Historical-ssp585 ()	reasonable	reasonable	0.281 (0.223 ... 0.331)	-0.17 (-0.65 ... 0.20)	51.251
CNRM-CM6-1 Historical-ssp585 ()	reasonable	reasonable	0.410 (0.307 ... 0.503)	-0.22 (-0.72 ... -0.058)	48.748
EC-Earth3-Veg-LR Historical-ssp585 ()	good	reasonable	0.455 (0.317 ... 0.549)	-0.054 (-0.43 ... 0.31)	31.521
EC-Earth3-Veg Historical-ssp585 ()	reasonable	reasonable	0.459 (0.356 ... 0.539)	-0.23 (-0.77 ... 0.018)	30.808
EC-Earth3 Historical-ssp585 ()	reasonable	reasonable	0.348 (0.269 ... 0.444)	-0.41 (-1.1 ... -0.18)	31.937
FGOALS-g3 Historical-ssp585 ()	good	bad	0.396 (0.302 ... 0.462)	0.23 (-0.073 ... 0.53)	28.15
INM-CM4-8 Historical-ssp585 ()	bad	bad	0.472 (0.350 ... 0.543)	0.35 (0.049 ... 0.87)	16.988
INM-CM5-0 Historical-ssp585 ()	reasonable	bad	0.413 (0.298 ... 0.508)	0.57 (-0.13 ... 1.2)	21.257
MIROC6 Historical-ssp585 ()	good	bad	0.376 (0.302 ... 0.438)	-0.20 (-0.83 ... 0.13)	31.730
MPI-ESM1-2-HR Historical-ssp585 ()	reasonable	bad	0.393 (0.295 ... 0.468)	-0.023 (-0.32 ... 0.28)	24.918
MPI-ESM1-2-LR Historical-ssp585 ()	bad	bad	0.533 (0.377 ... 0.664)	-0.047 (-0.54 ... 0.14)	27.321

MRI-ESM2-0 Historical-ssp585 ()	good	reasonable	0.340 (0.248 ... 0.398)	-0.082 (-0.42 ... 0.14)	35.423
NorESM2-LM Historical-ssp585 ()	bad	bad	0.501 (0.393 ... 0.579)	0.13 (-0.39 ... 0.63)	15.025
NorESM2-MM Historical-ssp585 ()	bad	bad	0.410 (0.311 ... 0.477)	0.33 (-0.042 ... 0.77)	26.647
TaiESM1 Historical-ssp585 ()	bad	bad	0.483 (0.356 ... 0.590)	-0.16 (-0.59 ... 0.025)	34.138

4.2 For Libya region

Table 2*: Evaluation results for the climate models considered for the attribution analysis of the annual (July-June) maximum 1-day rainfall for the Libya study region. The table contains qualitative assessments of seasonal cycle and spatial pattern of precipitation from the models (good, reasonable, bad) along with estimates for dispersion parameter, and event magnitude. The corresponding estimates for the ERA5 dataset is shown in blue. Based on overall suitability, the models are classified as good, reasonable and bad, shown by green, yellow and red highlights, respectively.*

Observations	**Seasonal cycle**	**Spatial pattern**	**Dispersion**	**Shape parameter**	**Event magnitude**
ERA5			0.422 (0.349 ... 0.475)	0.20 (-0.050 ... 0.36)	
Model					**Threshold for 1-in-600 year event**
CNRM-CM5_r1_ALADIN53 ()	bad	bad	0.376 (0.276 ... 0.442)	0.27 (-0.033 ... 0.78)	41.9339297
CNRM-CM5_r1_ALARO-0 ()	reasonable	good	0.306 (0.179 ... 0.408)	0.74 (0.13 ... 1.8)	58.8764549
CNRM-CM5_r1_CCLM4-8-17 ()	good	good	0.404 (0.293 ... 0.485)	0.41 (0.14 ... 0.76)	91.639945
CNRM-CM5_r1_RACMO22E ()	good	reasonable	0.419 (0.273 ... 0.497)	0.48 (0.066 ... 1.2)	77.4255125
CNRM-CM5_r1_REMO2015 ()	good	reasonable	0.322 (0.235 ... 0.385)	0.36 (0.064 ... 0.76)	33.8263098
EC-EARTH_r1_COsMO-crCLIM-v1-1 ()	reasonable	good	0.439 (0.335 ... 0.504)	0.28 (-0.040 ... 0.73)	31.0169627
EC-EARTH_r1_RACMO22E ()	bad	reasonable	0.402 (0.299 ... 0.474)	0.35 (0.0087 ... 0.73)	31.412888
EC-EARTH_r12_RACMO22E ()	reasonable	reasonable	0.343 (0.250 ... 0.400)	0.21 (-0.021 ... 0.47)	27.4117549
EC-EARTH_r3_RACMO22E ()	good	reasonable	0.416 (0.316 ... 0.490)	0.46 (0.12 ... 0.80)	62.4850852
HadGEM2-ES_r1_COsMO-crCLIM-v1-1 ()	reasonable	good	0.357 (0.269 ... 0.408)	0.16 (-0.15 ... 0.44)	20.6028273
HadGEM2-ES_r1_RACMO22E ()	reasonable	reasonable	0.252 (0.183 ... 0.307)	0.48 (0.17 ... 0.81)	33.8393727
IPSL-CM5A-MR_r1_REMO2015 ()	good	bad	0.378 (0.241 ... 0.456)	0.16 (-0.34 ... 0.72)	16.4569715
MPI-ESM-LR_r1_RACMO22E ()	reasonable	reasonable	0.293 (0.208 ... 0.351)	0.13 (-0.12 ... 0.39)	26.8694078
MPI-ESM-LR_r1_REMO2009 ()	reasonable	bad	0.316 (0.227 ... 0.375)	0.14 (-0.12 ... 0.46)	23.932556

MPI-ESM-LR_r2_COsMO-crCLIM-v1-1 ()	reasonable	good	0.374 (0.301 ... 0.424)	-0.085 (-0.56 ... 0.30)	24.9667883
MPI-ESM-LR_r2_REMO2009 ()	reasonable	bad	0.298 (0.209 ... 0.385)	0.12 (-0.46 ... 0.48)	23.6586723
MPI-ESM-LR_r3_REMO2015 ()	good	bad	0.263 (0.175 ... 0.351)	0.52 (-0.056 ... 0.92)	67.9642204
NorESM1-M_r1_ALADIN63 ()	bad	bad	0.360 (0.277 ... 0.405)	0.0047 (-0.28 ... 0.28)	19.5914793
NorESM1-M_r1_COsMO-crCLIM-v1-1 ()	bad	reasonable	0.405 (0.304 ... 0.473)	0.29 (0.020 ... 0.75)	28.032721
NorESM1-M_r1_RACMO22E ()	good	reasonable	0.307 (0.233 ... 0.366)	0.29 (-0.095 ... 0.64)	25.7074147
NorESM1-M_r1_REMO2015 ()	reasonable	bad	0.355 (0.255 ... 0.425)	0.18 (-0.044 ... 0.43)	21.6532809
CNRM-CM6-1-HR ()	reasonable	reasonable	0.300 (0.248 ... 0.341)	0.051 (-0.16 ... 0.20)	65.66
MPI-ESM1-2-HR ()	reasonable	reasonable	0.351 (0.291 ... 0.400)	-0.043 (-0.21 ... 0.094)	36.621
HadGEM3-GC31-MM ()	good	reasonable	0.333 (0.248 ... 0.393)	0.20 (-0.091 ... 0.68)	84.79
CMCC-CM2-HR4 ()	good	reasonable	0.290 (0.211 ... 0.351)	0.24 (0.16 ... 0.57)	77.34

5 Multi-method multi-model attribution

5.1 For GBT region

Table 3. *Probability ratio and change in intensity for models that passed the validation tests, for the GBT region.*

	a. Past vs. present		**b. Present vs. future**	
Model / Observations	**Probability ratio PR [-]**	**Change in intensity ΔI [mm/day]**	**Probability ratio PR [-]**	**Change in intensity ΔI [%]**
ERA5	5.0 (0.64 ... 1.1e+2)	32 (-5.5 ... 86)		
CMCC-CM2-HR4 SST-present (1)	1.2 (0.11 ... 15)	2.3 (-21 ... 38)		
CNRM-CM6-1-HR SST-present (1)	0.97 (0.21 ... 1.2e+2)	9.4 (-18 ... 43)		
HadGEM3-GC31-MM SST-present (1)	0.61 (0.079 ... 4.8)	-8.7 (-33 ... 24)		
MPI-ESM1-2-HR SST-present (1)	7.4 (0.59 ... ∞)	30 (-5.2 ... 71)		
AM2.5 amipHistorical+rcp4.5SST (3)	0.84 (0.44 ... 1.5)	-3.6 (-15 ... 8.9)	0.82 (0.68 ... 0.97)	-4.2 (-7.9 ... -0.64)
CNRM-CM5_r1_RACMO22E Historical-rcp85 ()	1.0 (0.21 ... 4.5)	0.17 (-23 ... 28)	1.0 (0.57 ... 1.6)	0.72 (-8.7 ... 8.3)

EC-EARTH_r1_RACMO22E Historical-rcp85 ()	0.50 (0.21 ... 1.1)	-17 (-35 ... 2.5)	1.1 (0.77 ... 1.5)	2.1 (-5.9 ... 9.3)
EC-EARTH_r3_COsMO-crCLIM-v1-1 Historical-rcp85 ()	0.53 (0.097 ... 2.0)	-15 (-41 ... 19)	0.60 (0.31 ... 0.97)	-13 (-25 ... -0.63)
HadGEM2-ES_r1_COsMO-crCLIM-v1-1 Historical-rcp85 ()	1.9 (0.15 ... 5.4)	12 (-15 ... 45)	1.4 (0.86 ... 1.8)	8.1 (-3.3 ... 17)
HadGEM2-ES_r1_RACMO22E Historical-rcp85 ()	0.59 (0.092 ... 1.8)	-12 (-34 ... 20)	1.1 (0.76 ... 1.3)	1.6 (-6.6 ... 9.8)
MPI-ESM-LR_r1_RACMO22E Historical-rcp85 ()	0.73 (0.17 ... 2.7)	-5.6 (-24 ... 22)	0.94 (0.43 ... 1.5)	-1.1 (-11 ... 7.9)
MPI-ESM-LR_r1_REMO2009 Historical-rcp85 ()	0.72 (0.089 ... 2.9)	-7.5 (-33 ... 29)	0.56 (0.19 ... 1.1)	-13 (-28 ... 1.5)
MPI-ESM-LR_r2_COsMO-crCLIM-v1-1 Historical-rcp85 ()	0.72 (0.17 ... 2.3)	-8.5 (-38 ... 25)	0.66 (0.33 ... 1.0)	-10 (-26 ... 1.2)
MPI-ESM-LR_r3_REMO2015 Historical-rcp85 ()	0.98 (0.28 ... 3.1)	-0.56 (-24 ... 28)	0.88 (0.57 ... 1.2)	-3.0 (-12 ... 4.6)
NorESM1-M_r1_RACMO22E Historical-rcp85 ()	0.71 (0.0 ... 10)	-6.4 (-41 ... 44)	0.82 (0.20 ... 1.4)	-3.5 (-14 ... 7.5)
ACCESS-CM2 Historical-ssp585 ()	1.4 (0.34 ... 4.5)	6.8 (-14 ... 34)	0.83 (0.45 ... 1.4)	-3.4 (-13 ... 6.9)
EC-Earth3-Veg-LR Historical-ssp585 ()	1.3 (0.39 ... 3.4)	4.8 (-15 ... 27)	0.92 (0.52 ... 1.3)	-1.5 (-10 ... 5.8)
MRI-ESM2-0 Historical-ssp585 ()	0.61 (0.052 ... 1.9)	-8.0 (-27 ... 14)	0.99 (0.71 ... 1.2)	-0.26 (-4.7 ... 4.1)

5.2 For Libya region

Table 4. *Probability ratio and change in intensity for models that passed the validation tests, for Libya region.*

	a. Past vs. present		**b. Present vs. future**	
Model / Observations	**Probability ratio PR [-]**	**Change in intensity ΔI [mm/day]**	**Probability ratio PR [-]**	**Change in intensity ΔI [%]**
ERA5	3.0 (0.50 ... 2.1e+3)	29 (-11 ... 89)		
CNRM-CM5_r1_ALARO-0 ()	0.61 (0.32 ... 1.6)	-18 (-33 ... 13)	1.0 (0.77 ... 1.3)	0.66 (-7.7 ... 8.0)
CNRM-CM5_r1_CCLM4-8-17 ()	1.8 (1.0 ... 4.1)	36 (1.1 ... 95)	0.99 (0.81 ... 1.3)	-0.76 (-10 ... 12)

CNRM-CM5_r1_RACMO22E ()	0.91 (0.45 ... 5.1)	-3.8 (-32 ... 51)	0.87 (0.69 ... 1.1)	-6.8 (-19 ... 4.8)
CNRM-CM5_r1_REMO2015 ()	2.4 (0.81 ... 78)	24 (-4.4 ... 69)	1.3 (0.93 ... 1.9)	5.9 (-1.5 ... 13)
EC-EARTH_r1_COsMO-crCLIM-v1-1 ()	0.43 (0.015 ... 1.6)	-19 (-42 ... 14)	0.68 (0.30 ... 1.2)	-12 (-27 ... 3.5)
EC-EARTH_r12_RACMO22E ()	1.2 (0.060 ... 16)	3.2 (-22 ... 34)	1.3 (0.38 ... 5.9)	3.4 (-7.7 ... 13)
EC-EARTH_r3_RACMO22E ()	0.73 (0.32 ... 2.8)	-11 (-33 ... 27)	0.90 (0.62 ... 1.4)	-3.1 (-16 ... 8.8)
HadGEM2-ES_r1_COsMO-crCLIM-v1-1 ()	1.7 (0.56 ... 4.2e+2)	12 (-12 ... 46)	0.96 (0.63 ... 2.4)	-0.89 (-9.1 ... 8.2)
MPI-ESM-LR_r1_RACMO22E ()	1.4 (0.024 ... 64)	4.1 (-20 ... 39)	1.1 (0.45 ... 3.4)	1.6 (-8.0 ... 9.7)
MPI-ESM-LR_r2_COsMO-crCLIM-v1-1 ()	0.63 (0.077 ... 3.2e+2)	-7.9 (-27 ... 21)	0.92 (0.59 ... 4.9)	-1.8 (-16 ... 11)
NorESM1-M_r1_RACMO22E ()	1.7 (0.34 ... 94)	11 (-15 ... 48)	0.76 (0.52 ... 1.4)	-9.1 (-22 ... 6.1)
MPI-ESM1-2-HR ()	35 (0.60 ... ∞)	30 (-6.3 ... 79)	(...)	(...)
HadGEM3-GC31-MM ()	0.83 (0.18 ... 15)	-4.4 (-30 ... 36)	(...)	(...)
CMCC-CM2-HR4 ()	10 (2.0 ... ∞)	47 (13 ... 93)	(...)	(...)

6 Hazard synthesis

For this study we use two event definitions, capturing firstly the impacts of the flooding over Greece, Bulgaria and Türkiye resulting from 4 days of very heavy rainfall averaged over land in the GBT region defined in section 1.1 (36-42.5N, 20-28.5E). Given that the region receives little rain over the summer (JJAS) but much more in winter, we focus for this event on the 4-day max rainfall in JJAS. Secondly, we look at the 1-day maximum rainfall over the whole year in a smaller region over Libya (32-33N, 20-23E) where most of the heavy rain fell during this event and the flooding was severe. Although part of the same synoptic weather system and the resulting low-pressure system "Daniel", as described in the previous sections the rainfall characteristics in the two regions were quite different in temporal and geographical scale and with respect to return times, estimated to be around 10 years for the 4-day max JJAS rainfall in the larger GBT region and about 600 years for the 1-day maximum rainfall over the Libya region.

For both event definitions we evaluate the influence of anthropogenic climate change on the events by calculating the probability ratio as well as the change in intensity using observation-based products, in this case ERA5 reanalysis, and climate models. Models which do not pass the validation tests described in Section 4 are excluded from the analysis. The aim is to synthesise results from models that pass the evaluation along with the observations-based products, to give an overarching attribution statement. Figures 9-12 show the changes in probability and intensity in ERA5 (blue) and models (red). Before combining them into a synthesised assessment, a term to account for intermodel spread is added (in quadrature) to the natural variability of the models, if the intermodel spread is larger than that expected from sampling uncertainty. This is shown in the figures as white boxes around the light red bars. Given the large sampling uncertainty in the models these are quite small and hardly visible. The dark red bar shows the model average, consisting of a weighted mean using the (uncorrelated) uncertainties due to natural variability.

Observation-based products and models are combined into a single result in two ways. Firstly, we neglect common model uncertainties beyond the intermodel spread that is depicted by the model average, and compute the weighted average of models (dark red bar) and observations (dark blue bar): this is indicated by the magenta bar. Secondly, we also show the estimate of an unweighted, direct average of observations (dark red bar) and models (dark blue bar) contributing 50% each, indicated by the white box around the magenta bar in the synthesis figures. This second estimate places more weight on the observations than the first, which may be more appropriate in cases where, due to common model uncertainties, model uncertainty can be larger than the intermodel spread, and in particular for an event like this, where we know that models that do not resolve convection are not the ideal tools for this analysis.

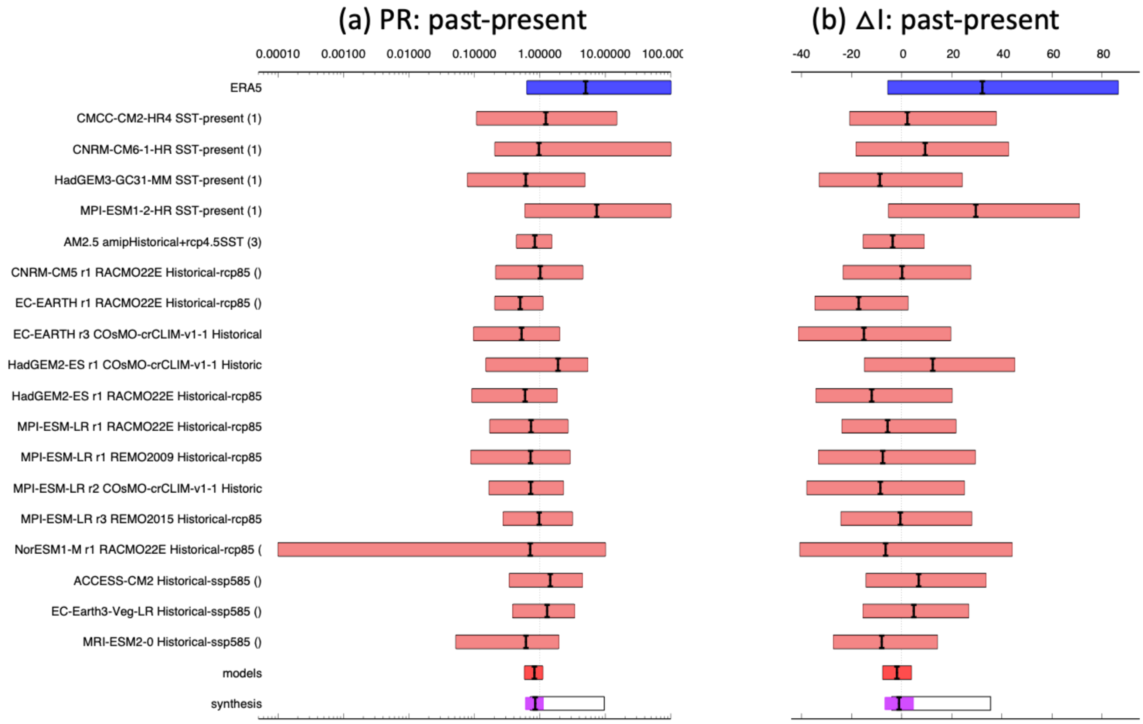

Figure 9: *Synthesis of (a) probability ratios and (b) intensity changes when comparing the return period and magnitudes of the 2023 JJAS seasonal Rx4day over the GBT region in the current climate and a 1.2°C cooler climate.*

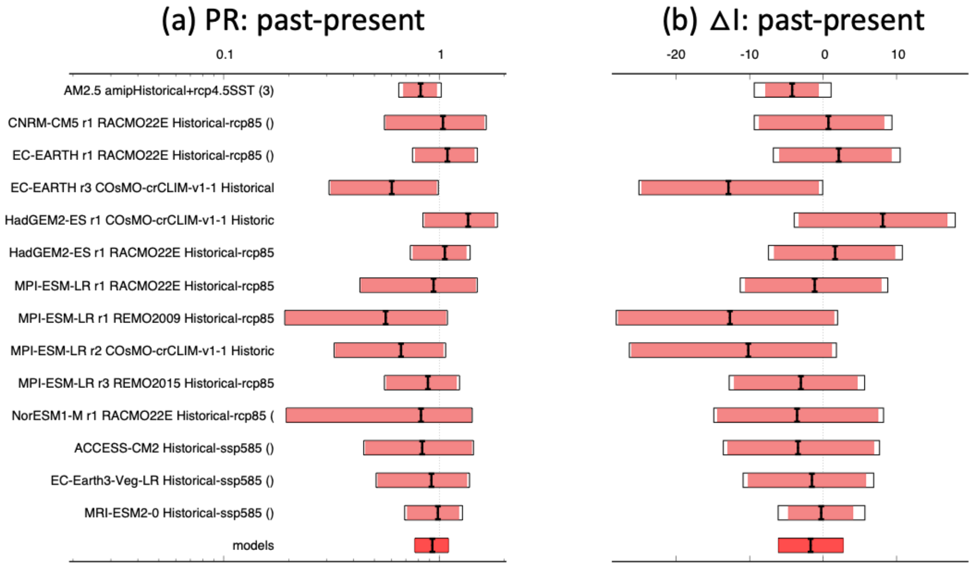

Figure 10: *As Figure 9 but for models only, of a 0.8°C warmer (2°C since pre-industrial) climate.*

Despite the different event definitions used, the results of the attribution analysis are very similar for both events. In both cases the best estimate of the model average and thus the weighted synthesised result is close to 1 for the probability ratio (PR), identifying no change in likelihood, and close to 0 for the change in intensity, albeit with large uncertainties. In contrast, the observation based product shows an increase in likelihood of the event, with a best estimate of 10 for the PR in case of the GBT-region and 3 for Libya. Similarly the best estimate shows an increase in intensity of about 30% for both regions, again with large uncertainties. This results in an unweighted synthesised probability ratio of 1 to 10 for the GBT region and 1 to 50 for Libya. The change in intensity is 0 to 36% for the GBT-region and 0 to 46% for Libya.

We report the unweighted range, giving models and observation based products equal weight, as our overarching results. While this choice includes the weighted average, and thus the possibility that human-induced climate change does not alter the likelihood and intensity in these events, it highlights that the likelihood could have increased by up to a factor of 10 and 50 respectively, and the intensity by up to around 36% and 46% in the GBT and Libya regions, respectively. From thermodynamic theory we know that an increase in intensity of 7% is to be expected with each 1°C of warming, so around 10% more precipitation would be expected given current warming levels, thus “no change” could only be confidently reported as the main result if there was a well known dynamic process counteracting this effect. While there are some papers exploring this (e.g. Brogli et al., 2019, Zittis et al., 2021), no conclusive results have been found. Furthermore studies focussing on extreme rainfall with future warming also show an increase in heavy rainfall on the 1 to 5-day timescale emerging (Zittis et al., 2022; Seneviratne et al., 2021), rendering it very plausible that the increase in the observation based product is indeed a trend due to climate change. The known fact that climate models with a resolution that requires convection to be parameterized are unlikely to be able to fully capture these events (Berg et al., 2019), particularly over Libya, further supports the decision to not give too much weight to the models and suggests the models could indeed not capture the process leading to the observed increase. The assessment of the models at 2°C of global warming thus does not add more information to the trends seen in ERA5 (Figures 11 and 12).

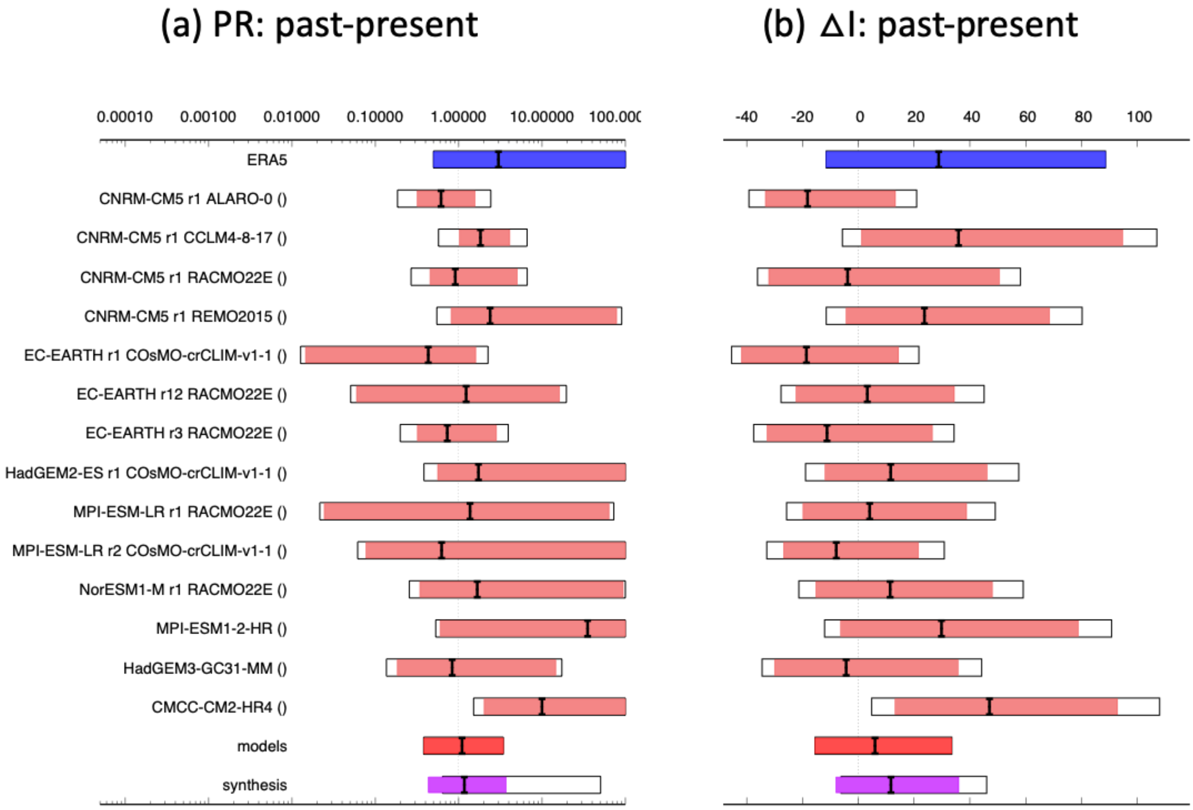

Figure 11: *Synthesis of (a) probability ratios and (b) intensity changes when comparing the return period and magnitudes of the 2023 annual (July-June) Rx4day over the Libya region in the current climate and a 1.2ºC cooler climate.*

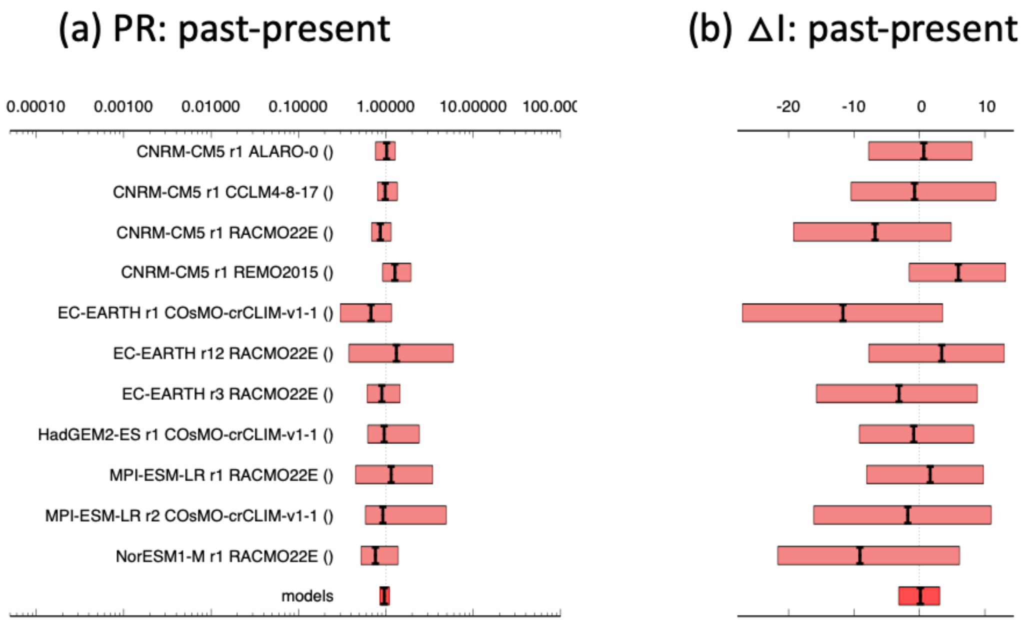

Figure 12: *As Figure 11 but for models only, of a 0.8ºC warmer (2ºC since pre-industrial) climate.*

Combining lines of evidence from the synthesis results of the past climate, results from future projections reported in the IPCC and physical knowledge we communicate the probability ratio of 1 to 10 for the GBT region and 1 to 50 for Libya. The change in intensity is 0 to 40% for the GBT-region and 0 to 50% for Libya as the overarching result.

7 Vulnerability and exposure

Risk is more than simply the hazard or meteorological conditions that occur. Disasters occur when this hazard interacts with exposed regions, and assets, and with vulnerable human, political, and economic systems (IPCC, AR6).

Storm Daniel brought extreme rainfall and flooding to Greece, Türkiye, Bulgaria, and Libya. The floods at study here are already the costliest weather-related disaster of 2023, and are amongst the deadliest flood-related events on record with at least 3,958 people confirmed dead and 20,000 families displaced in Libya (Al Jazeera, 2023). The extensive and intensive impacts that are still being experienced at the time of writing and are a product of both the highly unusual amount of rain that fell, and infrastructure and systems that were unable to withstand the hazard. These floods follow a summer of extreme weather in the form of heatwaves, unprecedented wildfires, and drought across the Mediterranean, with Greece having also dealt with the EU's biggest-ever wildfire in the northeast of the country (European Commission, 2023). In Libya the disaster was compounded by the ongoing conflict situation, and cascading impacts such as landslides.

In the following sections, we provide a review of the vulnerability and exposure factors that contributed to or alleviated the impacts of the floods with a focus on Greece and Libya. To fully understand the drivers of the disaster, after-action reviews and post-disaster research will be essential to fill in the gaps in knowledge that currently exist and to inform improved disaster preparedness, and adaptation planning.

7.1 Land-use management and urban planning

The extent and impact of floods is mediated by the changes humans make to the environment, including land-use and land cover changes, the building of infrastructure (e.g. buildings, roads, dams etc.), that may block or channel the water, and urban planning decisions that govern some of these changes in urban areas.

7.1.1 Greece

In Greece, the centre of the country was most affected by the floods, including the agricultural Thessaly plain where 16 people died, crops were damaged, animals drowned, and hundreds of people required rescue (AP News, 2023). While Greece has no megacities, urbanisation has grown rapidly in the country with 80% of the population living in cities and villages, up from only 56% in 1960 (UN Population Division, 2018). When extreme rainfall occurs, like in this event, the changes to the landscape, including conversion of agricultural land to village or city land, deforestation, and the building of roads, homes, and bridges, has an impact on where stormwater runoff is able to go and often creates locally higher flood levels due to water being channelised in certain areas (Angelakis et al., 2019).

7.1.2 Libya

Since the discovery of oil in the 1950s, Libya has undergone rapid urbanisation, with the availability of water dictating where the concentration of people could reside (Mahmoud-Misrati, 1983). The city of Derna, Libya where preliminary evidence suggests two dams failed leading to the vast majority of casualties, was densely populated with settlements along the river that satellite imagery of the aftermath of the floods shows were destroyed due to the impact to the floods (Planet SkySat, 2023). Preliminary estimates indicate that 2,217 buildings were exposed to rushing water (UNITAR and UNOSAT, 2023).The sheer volume of water released from the dams swept away much of the infrastructure in its path. Across Libya, conflict and related poor operations and maintenance has resulted in damage and destruction to physical infrastructure (Irhiam, 2023). Since 2014 the city of Derna, has been controlled by a number of different groups including militants associated with the Islamic State (IS), and is currently under the control of the Libyan National Army under Khalifa Haftar (Annahar, 2023). In addition, a long-term decline in rainfall has also contributed to increasingly compacted soils, limiting the ability of water to penetrate into the ground and instead increasing runoff during heavy rainfall events (Ashoor, 2022).

7.2 Conflict and displacement

7.2.1. Governance and conflict

Since 2011, Libya has been a state in conflict, and undergoing a large humanitarian crisis (ACLED, 2019). The Arab Spring protests of 2011, two civil wars and international intervention that followed, cycles of ceasefires and fighting, government changes and instability, have characterised the political and humanitarian context of the country and the backdrop in which these disastrous floods occurred. The political map of Libya is complex as well - the city of Derna, which saw most of the casualties from these floods, is currently under control of the Libyan National Army (LNA) with significant rifts and instability. For instance, municipal elections scheduled for September 2023 were canceled by clashes and pressure from armed forces loyal to the LNA (The Libya Observer, 2023; Le Monde, 2023). This unstable political situation has been pointed by many as a cause of the lack of disaster preparedness, and hampering disaster response capacity (CNN, 2023).

7.2.2. Migration and Displacement

Human mobility including migration and displacement has many reasons. Drivers of social, economic, institutional, and physical vulnerability in the face of weather-related disasters can lead people to move temporarily, for example over short distances, out of harm's way. When faced with extreme weather events, conflict situations can be amplified and in rare cases, leading people not only move short distances but also seek refuge in neighbouring countries (Brzoska, 2018; Mach et al., 2019; Missirian and Schlenker, 2017).

Libya is one of the top countries seeking refugee status in Europe. In November and December 2023, the International Organization for Migration (IOM) counted close to 700,000 migrants, a number that has been steadily growing since the pause of the Covid-19 pandemic (IOM, 2023). Displacement and migration is multicausal (McLeman et al., 2019). In Libya, decades of political instability and conflict have internally displaced large portions of the population (IDMC, 2023). Migrant and/or refugees departing from Libya also live in states of economic and political precarity, with limited services, information, and support (UNHCR, 2021). Prior to Storm Daniel, the Derna region hosted an estimated 46,000 internally displaced people (IDPs) (Al Jazeera, 2023). According to UNHCR, the September 2023 storm added around 30,000 IDPs to the Derna region and an additional 8,640 IDPs are estimated to live in precarious locations around the coastline and neighbouring districts, in camps or peri-urban settings (IOM DTM, 2023; MapAction, 2023). Even though these numbers are likely an underestimation, displacement estimates should be seen in the wider context of caveats in data collection, displacement as a coping mechanism and those individuals who lack the ability to move when faced with extreme weather (Buhaug, 2023; Cundill et al., 2021).

The vulnerability of a person affects their ability to respond to risk, which may be categorised into various types, such as socio-economic, physiological, attitudinal, and institutional vulnerability (Adger, 2006). Communities experiencing displacement will have significantly and disproportionately been impacted by the September 2023 floods, both in Libya and across the Mediterranean in Europe (IOM, 2023). In Greece, for example, the Thessaly region that was worst-affected by the floods has a large undocumented migrant population, many of whom are employed in the agricultural industry which was severely impacted by the floods (Kapsalis, 2022). Since 2015, Greece has also been hosting a disproportionately large number of EU-bound migrants (MPI, 2020). However, the number of people seeking refuge in Italy, Malta or Greece has decreased significantly (2022: 159,410 refugees) compared to the peak years of 2015 (1,032,408 refugees) (UNHCR, 2023). Within the affected regions, disparities in socio-economic factors influence who is at the forefront of flood risk and associated impacts (Kruczkiewicz et al., 2022; Thalheimer et al., 2022). People who live in places where they have language barriers, limited social networks, lack local knowledge about risk and response action, are not connected to information systems or accounted for in government response systems, are highly vulnerable to disasters (Benveniste et al., 2020). Elderly and children, people with disabilities, existing illnesses, medical conditions, and/or dependencies on external aid, including mental health issues are considered to be at higher risk, for example due to decreased ability to move out of harm's way (Benveniste et al., 2023).

Flood impacts can be exacerbated by lack of financial or social resources, limited well-being, lack of awareness and/or information received. For example, in Derna, Libya 50% of households are considered "poor" or "near poor" impacting their exposure to flood hazards, and ability to recover (UNESCWA, 2015). Such factors are often determined by wider social, economic, and political systems, and intersect in complex ways. On the other hand, having good capacities to respond to this flood risk might not have been enough to mitigate the loss and damages with an event of this severity.

7.3 Dam failures in Libya

Built in the 1970s, the Abu Mansour and Al-Bilad dams were constructed to help protect Derna from the floods that had previously devastated the city in 1941, 1956, 1959, 1968, and 1989, as well as providing water for agriculture (News Libya, 2023). The 70-meter tall upper dam, Al-Bilad, had the storage capacity of 1.5 million cubic meters, while the lower, Abu Mansour, had one of 22.5 million cubic meters (EOS, 2023). When Al-Bilad burst at approximately 02:30 am on the morning of 11 September, the accumulated water rushed downstream and overwhelmed Abu Mansour to the point of collapse (Al Jazeera, 2023). Located merely one kilometer above Derna, the three to seven meter high flash floods unleashed subsequently tore through the city (CNN, 2023; EOS, 2023; IFRC, 2023).

Libya is one of the most water scarce countries in the world with very limited rainfall and The Great Man-Made River Project developed to bring water to coastal areas (World Bank, 2023). Therefore, its not surprising that the country's focus is primarily to manage water resources to ensure there is enough water for agriculture and the population needs, rather than low-likelihood flood events. Preliminary reports indicate that both dams may not have been built to withstand the volumes of rainfall that fell over the largely arid Northeastern Libya, and state fragility had moreover severely limited the maintenance of the dam system since 2002 (Ashoor, 2022; University of Reading, 2023; Al Jazeera, 2023a; Al Jazeera, 2023b). The dam design relied on relatively short rainfall time series data and therefore may not accurately taken into account the "probable maximum flood" which is considered the standard for dam safety (Ashoor, 2022; FERC, 2004). Critically, last year, Ashoor (2022) published a scientific paper spotlighting the hydrological risks to the dams and the urgent need for periodic maintenance in order to avoid a high flood risk in the Wadi Derna basin. Further post-disaster investiagtions and reviews will be required to pinpoint the extent to which the dam design, extreme rainfall, safety features (or lack thereof) and maintenance over time contributed to the disaster. Going forward, the city will likely need to build new flood protection infrastructure (which may include dams) that should take into account the changing risk of extreme rainfall events in the current and future climate.

7.4 Disaster risk management

7.4.1 Flood protection and adaptation

In Greece, the Ministry of Environment and Energy is responsible for coordinating the country's climate change mitigation and adaptation work. In 2016, Greece adopted its National Adaptation Strategy, whose key objectives include establishing and strengthening decision-making, policy-making, action, and a monitoring and evaluation mechanism for adaptation, linking this work with commitments towards the Global Goals, as well as promoting public awareness and capacity around adaptation (Hellenic Republic, 2018). Further, it outlines the requirements for all 13 Regional Authorities to develop Regional Adaptation Action Plans during its first policy cycle (2016-2025).

In 2017, Greece's first nation-wide flood hazard map identified that 24% of the country is under "very high" flood risk (Kourgialas & Karatzas, 2017). Since then, flood hazard maps have been developed for all areas of the country (Hellenic Association of Insurance Companies, 2018). While 80% of Greece's urban areas and half of its road network are located in flood-prone areas, the lowlands and slopes, rapid urbanization, and large burned areas in the South and East render them to constitute particular hotspots for flood risk (Skilodimou et al., 2021).

A pre-feasibility study was conducted in 2022 on the use of a number of nature-based solutions (NbS) to reduce flood risk in the heavily flood-affected region of Thessaly (WWF Greece, 2022). The study confirmed the viability and effectiveness of the piloted measures, including restoring natural water retention ponds, wetlands and floodplains, and a range of urban greening strategies, and put forth a suggested roadmap for a regional programme for NbS implementation. Another study led by Spyrou et al. (2022) concluded that the construction of a flood storage reservoir was successful in reducing flood risk in the Spercheios river basin.

In Libya, the complex political and economic challenges experienced post 2011 have significantly constrained the country's progress in addressing its vulnerability to climate change through adaptation and disaster risk reduction plans, along with having prevented the roll-out of a national development plan (United Nations Libya, 2022). The country is yet to develop a National Adaptation Plan, and in 2016, Libya indicated governance issues as the main challenge standing in their way (UNFCCC, 2016). To date, it is also the nation which has accessed least funding from the Green Climate Fund (UNFCCC, 2021). UNDP is supporting Libya to raise public awareness, foster institutional capacity, and engage with multilateral climate actors (IOM, 2022).

7.4.2 Early warning early action

On 1 September, the Hellenic National Meteorological Service issued an orange weather alert to notify the public of the forecast torrential rainfall (Crisis24, 2023). The day before the heaviest rainfall started, on 3 September, the warning was upgraded to a red alert (MeteoAlarm, 2023), which is the highest level, and the authorities sent push alerts to cell phones instructing people to avoid the outdoors (Greek City Times, 2023). Based largely on the warnings, over 5,260 people were evacuated across the rainfall-affected regions of Thessaly, Central Macedonia, Peloponnese, and Attica - over half of which (at least 3,500) took place in the former (ECHO, 2023). In Thessaly's capital, Larissa, city authorities preemptively placed sandbags and pebbles along the rapidly swelling River Pineios, while also opening up diversion channels located west of the city, but could not prevent it from overflowing (VOA News, 2023).

Leaving the Balkan Peninsula, the storm track of Medicane Daniel was well-forecast for Libya. Numerical weather prediction model forecasts also indicated very heavy rainfall over Libya. Three days before the heavy rainfall hit northeastern Libya, the National Meteorological Centre issued early warnings, notifying all government authorities and urging them to roll out preventive measures (WMO, 2023). The day before the storm struck, a warning on the weather conditions was issued to people in Derna and surrounding cities by the office of Osama Hamad, which moreover declared a preemptive state of emergency (CNN, 2023; Ahram Online, 2023). The warnings were reportedly poorly disseminated and were issued by more than one authority, which may have also led to conflicting warning messages (Reuters, 2023). In addition, there is often a risk perception gap when only meteorological information is shared, as those receiving the warnings do not understand how the weather is expected to interplay with the environment, and impact people, assets, livelihoods and infrastructure. Impact-based weather forecasts and warnings can help to close the gap by linking the hazard forecast with vulnerability and exposure factors that help emergency managers and others understand the tangible risks associated with the weather (WMO, 2018).

The catastrophic human toll of the floods is directly linked to the failure of the two dams located upstream of Derna (CNN, 2023; Reuters, 2023). Important to note is that the city of Derna had no evacuation plans in place to support early action based on a forecast of extreme weather (AP News, 2023). Considering that the high volume and speed of the flash floods making mere exposure likely lethal, preemptively removing people from the water's pathway would have saved lives.

7.4.3 Response, Relief, and Recovery

In Greece, the Hellenic Red Cross assisted in evacuations, provided first aid to injured people, transported patients to hospitals, and distributed potable water and food (IFRC, 2023a). The regional Red Cross branch in Larissa moreover provided psychosocial support to affected populations as well as dispatched social welfare volunteers to assist in the flood-affected areas (IFRC, 2023a). In response to the widespread devastation in Thessaly, Greece's Prime Minister has stated that the country will seek funds from the EU Solidarity Fund and the Recovery Fund, as well as a loan from the European Investment Bank (EU Observer, 2023).

According to IFRC (2023b), the disaster in Libya has directly affected 1.6 million people, and it is targeting 200,000 for humanitarian assistance over the coming three months to support people and households whose homes were destroyed and livelihoods impacted. The appeal of 10 million Swiss franc includes integrated response, in part with the objective to develop early warning early action activities (IFRC, 2023b). OCHA (2023) has also launched a flash appeal of $71.4 million, targeting roughly 250,000 people in the region of nearly 900,000 affected. To date, disaster response has been hampered by disruptions in transportation infrastructure which delay humanitarian assistance from reaching those most affected. In the aftermath of the floods, people lack access to basic services such as electricity, clean water, shelter, food, and there is a large potential for the spread of waterborne illness and disease, underscoring the enormous challenge ahead (Guardian, 2023).

7.5 V&E Conclusions

In Greece, this has been a summer of extreme heatwaves and in the northeast of the country one of the largest fires was burning as Storm Daniel devastated the centre of the country, stretching resources and limiting country-level response capabilities. Deforestation and relatively high rates of urbanisation have changed the landscape over time, increasing the number of people and assets exposed to flooding, and reducing stormwater drainage.

In Libya, the volume of water and overnight timing of the dam failures made it so that anyone in the path of the water was at increased risk, not just those who are typically highly vulnerable. Ongoing conflict and state fragility in Libya compounded the effects of the flooding, contributing to a lack of maintenance and deterioration of dam infrastructure over time and increasing people's risk and the resulting impacts. The conflict also limits nation-wide adaptation planning and coordination across a range of climate issues facing the country, such as water scarcity, and extreme weather including heat and floods.

In addition to the lack of maintenance, the Al-Bilad and Abu Mansour dams were built in the 1970s, using relatively short rainfall records, and may not have been designed to withstand a 1 in 600 year rainfall event. A full after-action review looking at the design criteria of the dams will be required to understand the extent to which the dams' design, and the lack of subsequent maintenance contributed to the disaster. Even still, catastrophic dam failures and its impacts can be limited through risk reduction protocols that include real-time monitoring of forecasts, water volumes, and warning systems that alert those downstream of possible failures and the need to evacuate. While in Libya there was a forecast with a 3-day lead time on the track of Storm Daniel, the impact of that potential rainfall on infrastructure and people was not clearly understood in advance. Further, it is not clear to what extent forecasts and warnings were communicated and received by the general public, or relevant emergency responders. In conjunction with improved emergency management capacity, impact-based forecasts may help to provide a clearer understanding of how the rainfall translates into potential impacts and could lead to improved warnings in the future.

This disaster also points to the challenge of needing to design and maintain infrastructure for not just the climate of the present or the past, but also the future. In Libya, this means taking into account the long-term decline in *average* rainfall, and at the same time, the increase in *extreme* rainfall like this heavy rainfall event; a challenging prospect especially for a country plagued by crises.

Data availability

Almost all data are or will soon be available via the Climate Explorer.
For station data from the National Observatory of Athens, please contact Vassiliki Kotroni (kotroni@noa.gr) *and* Lagouvardos Kostas (lagouvar@noa.gr).

References

All references are given as hyperlinks in the text.